Chemical Science

ROYAL SOCIETY OF CHEMISTRY

EDGE ARTICLE

View Article Online
View Journal | View Issue

Cite this: *Chem. Sci.*, 2024, **15**, 1088

All publication charges for this article have been paid for by the Royal Society of Chemistry

Negative to positive axial thermal expansion switching of an organic crystal: contribution to multistep photoactuation†

Shodai Hasebe, ‡[a] Yuki Hagiwara, ‡[a] Takashi Ueno,[b] Toru Asahi[abc] and Hideko Koshima *[c]

Materials displaying negative thermal expansion (NTE), in contrast to typical materials with positive thermal expansion (PTE), are attractive for both fundamental research and practical applications, including the development of composites with near-zero thermal expansion. A recent data mining study revealed that approximately 34% of organic crystals may present NTE, indicating that NTE in organic crystals is much more common than generally believed. However, organic crystals that switch from NTE to PTE or *vice versa* have rarely been reported. Here, we report the crystal of *N*-3,5-di-*tert*-butylsalicylide-3-nitroaniline in the enol form (enol-**1**) as the first organic crystal in which the axial thermal expansion changes from negative to positive at around room temperature. When heated, the crystal shrinks along the *a*-axis below 30 °C and then it expands above 30 °C. Geometric calculations revealed that below 30 °C, the decrease in the tilt angle of the molecule exceeds the increase in the interplanar distance, causing NTE, whereas above 30 °C, the increase in the interplanar distance outweighs the decrease in the tilt angle, resulting in PTE. By combining photoisomerisation and the NTE–PTE switching induced by the photothermal effect, multistep crystal photoactuation was achieved. Moreover, actuation switching of the same crystal sample by changing atmosphere temperature was realised by utilising the NTE–PTE change. Such NTE–PTE switching without a thermal phase transition provides not only new insight into organic crystals but also a new strategy for designing crystal actuators.

Received 12th September 2023
Accepted 10th December 2023

DOI: 10.1039/d3sc04796b

rsc.li/chemical-science

Introduction

Thermal expansion is a fundamental property of solids. Most materials expand on heating and undergo positive thermal expansion (PTE) in all directions due to an increase in the interatomic bond length, which is caused by increasing the anharmonic vibrational amplitudes of atoms.[1] However, some materials show the opposite effect, known as negative thermal expansion (NTE). NTE has been discovered mainly in framework structure materials, for instance oxides, cyanide, and metal–organic frameworks (MOFs), in which the relatively large void space and flexible bridging linkage units promote the transverse vibration of atoms to trigger NTE.[2]

Besides framework structure materials, some organic molecular crystals, in which molecules are connected by non-covalent intermolecular interactions, have been reported to exhibit either uniaxial or biaxial NTE.[3] For instance, the pentacene crystal shows uniaxial NTE by the increase in the herringbone angle caused by steric hindrance.[3c] The dumbbell-shaped (*S*,*S*)-octa-3,5-diyn-2,7-diol exhibits large uniaxial PTE and biaxial NTE caused by the tilting of molecules in the molecular columns.[3d] Moreover, various mechanisms of NTE in organic molecular crystals have been elucidated in terms of distortion of linked rhombuses,[3e] layer sliding,[3f,h] and jack-like distortion.[3g] A recent data mining study indicates that approximately 34% of organic crystals may show NTE along at least one orthogonal axis, indicating that NTE in organic crystals is much more common than previously expected.[4] However, organic molecular crystals that switch from NTE to PTE or *vice versa* without a thermal phase transition have only rarely been reported.[5]

We focus on crystal actuation because mechanically responsive organic crystals that show macroscopic deformation upon external stimuli such as light and heat are not only

[a]*Graduate School of Advanced Science and Engineering, Waseda University, 3-4-1 Okubo, Shinjuku-ku, Tokyo, 169-8555, Japan*

[b]*Department of Nanoscience and Nanoengineering, Graduate School of Advanced Science and Engineering, Waseda University, 3-4-1 Okubo, Shinjuku-ku, Tokyo, 169-8555, Japan*

[c]*Research Organization for Nano & Life Innovation, Waseda University, 513, Waseda Tsurumakicho, Shinjuku-ku, Tokyo, 162-0041, Japan. E-mail: h.koshima@kurenai.waseda.jp*

† Electronic supplementary information (ESI) available: Detailed methods, crystallographic data (CIF and other formats), photoisomerisation properties, photomechanical motions, and movies. CCDC 2291942–2291949. For ESI and crystallographic data in CIF or other electronic format see DOI: https://doi.org/10.1039/d3sc04796b

‡ These authors contributed equally to this work.

intriguing for fundamental research but also fascinating candidates for sensors, actuators, and soft robots.[6] Various photomechanical (light-responsive) crystals have been reported, such as diarylethene,[7] azobenzene,[8] anthracene,[9] salicylideneaniline,[10] and others,[11] based mainly on photoisomerisation as well as photodimerization[9] and photopolymerisation.[11e] Thermal phase transition is a representative mechanism that actuates organic crystals by heat.[3g,12] Anisotropic thermal expansion without thermal phase transitions also triggers crystal actuation upon heating or cooling.[13] Recently, we discovered high-speed bending of crystals due to the photothermal effect,[14–17] by which heat is generated through the nonradiative deactivation of photoexcited materials. The photothermal effect increases the light-irradiated top surface temperature and elongates its length more than the back surface, resulting in a bending-away motion. Even though the deformations by the photothermal effect are small compared to those by photoisomerisation, the photothermal effect is advantageous in that it can achieve higher-speed actuation, a wider light wavelength range, the actuation of thicker crystals, and a broad variety of target materials.[6b,15] For instance, hybrid organic crystals coated with MXene—popular photothermal material with absorption from the UV to visible and near infrared region—can be actuated by the photothermal effect in a wide range of wavelengths from UV to visible[18b] and near infrared,[18] which is impossible by photoisomerisation. However, the bending behaviour has been limited to monotonous bending away[14,15,17] because typical organic crystals exhibit PTE over the entire temperature range. Organic crystals with NTE or PTE–NTE switching properties could diversify bending behaviour through the photothermal effect.

Salicylideneaniline derivatives are typical photochromic compounds that exhibit enol–keto photoisomerisation in the crystalline state.[19–21] Previously, we reported that thin (thickness $T < 10$ μm) crystals of *N*-3,5-di-*tert*-butylsalicylide-3-nitroaniline (**1**, Fig. 1a) in the enol form exhibit one-step bending-away motion due to photoisomerisation upon ultraviolet (UV) light irradiation as the first photomechanical salicylideneaniline crystal.[20] Recently, while investigating the two-step bending of enol-**1** crystals that were not thin ($T > 30$ μm) due to combined photoisomerisation and photothermal effects, we found that thick ($T > 100$ μm) crystals also undergo another new, small bending, achieving multistep bending (Fig. 1b). To clarify why the new bending occurred, we performed X-ray crystallographic analysis of enol-**1** crystals at different temperatures. We discovered that the thermal expansion of an enol-**1** crystal in the *a*-axis direction changes from negative to positive at around 30 °C as the temperature increases. We succeeded in reproducing the NTE–PTE switching of the *a*-axis length *via* a geometric calculation using the temperature dependence of both the interplanar distance and the tilt angle. The mechanism of the multistep bending of the thick enol-**1** crystal was explained by the photothermally induced NTE–PTE switching and photoisomerisation.

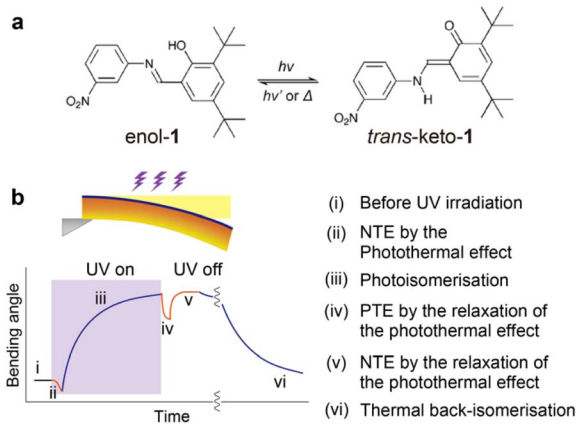

Fig. 1 (a) Enol–keto photoisomerisation of salicylideneaniline **1**. (b) Schematic illustrations of multistep bending of enol-**1** crystals by photoisomerisation and the photothermal effect.

Crystal structure

Enol-**1** was synthesised by the condensation of aldehyde and aniline (Fig. S1 and S2†). Plate-like crystals of enol-**1** were obtained by slow evaporation of methanol solutions at room temperature (Fig. 2a and b). Enol-**1** was crystallized in the space group $P\bar{1}$, with one molecule in the asymmetric unit, consistent with previous reports (Table S1†).[20,21] The molecule has a torsional conformation in which the salicyl and phenyl rings are not coplanar, and the conformation is anchored by intramolecular O–H···N hydrogen bonding (Fig. 2c and d). The enol-**1** molecules form dimers *via* intermolecular N–O···H–C=N interaction (I) between the nitro group and the Schiff base on the (100) face (Fig. 2e). The dimers are connected through intermolecular C–H···C–C interactions (II) between the neighbouring *tert*-butyl groups to form a 1D array along the *b*-axis.

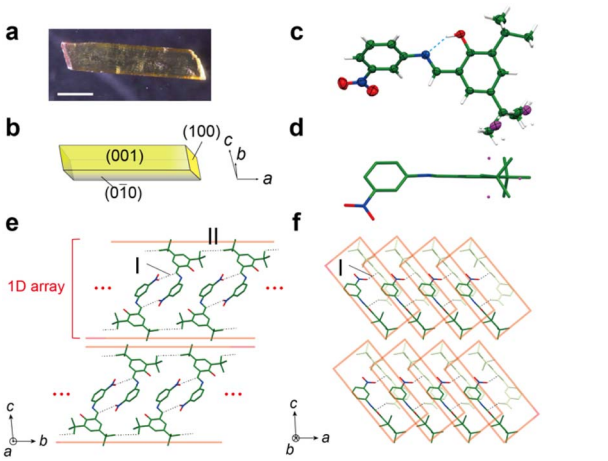

Fig. 2 Crystal structure of enol-**1** at 23.6 °C. (a) Photograph and (b) face indices. Scale bar: 1 mm. (c) Oak Ridge Thermal Ellipsoid Plot (ORTEP) drawings at 23.6 °C with a thermal ellipsoid of 25% probability. Disordered *tert*-butyl substituents are indicated in magenta. (d) Molecular conformation viewed perpendicular to the salicyl plane. Molecular arrangements on the (e) (100) and (f) (0$\bar{1}$0) faces. Intermolecular interactions I and II and 1D arrays are shown by dotted black lines and red lines, respectively. Hydrogen atoms and disordered structures are omitted for clarity.

Viewed from the (0$\bar{1}$0) face, the 1D arrays are tilted and stacked along the *a*-axis (Fig. 2f). The interaction between the 1D arrays along the *c*-axis is weak due only to weak van der Waals forces between the neighbouring *tert*-butyl groups (Fig. S6†).

Thermal expansion properties

Fig. 3 shows the temperature dependence of the lattice constants of the enol-**1** crystal from X-ray crystallographic analysis in the range from around 0 to 60 °C. Contraction of the *a*-axis was observed with increasing temperature until 30 °C, followed by expansion until the end of the experiment at 57 °C, showing switching from NTE to PTE (Fig. 3a). In contrast, the *b*- and *c*-axes showed the more usual expansion behaviour (Fig. 3b and c). In addition, the β-angle increased with temperature until 30 °C and then decreased, with an inflection point at around 30 °C (Fig. 3f and S7†). The α- and γ-angles decreased monotonically (Fig. 3e, g and S7†). Overall, the cell volume increased with temperature (Fig. 3d).

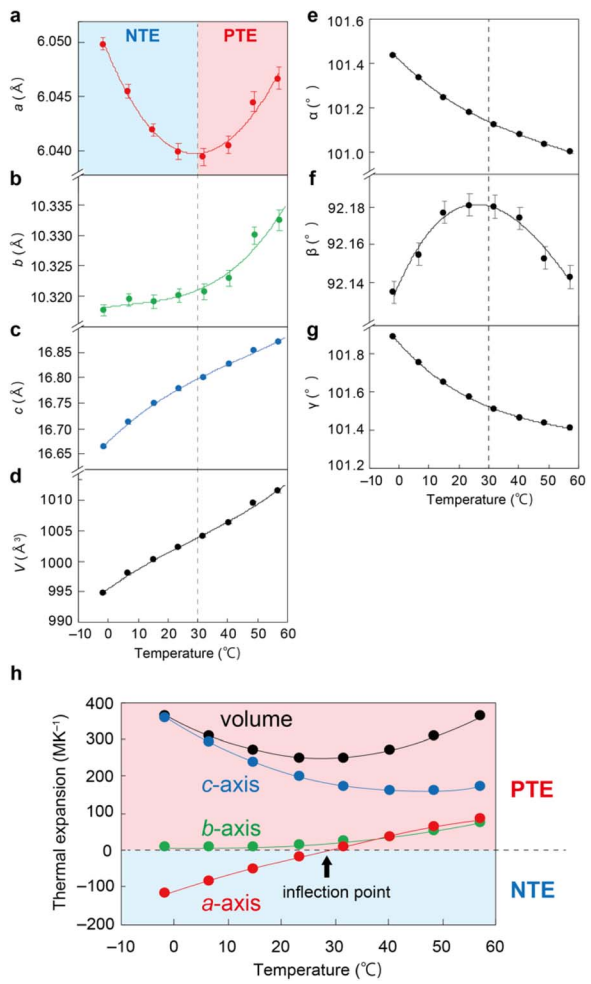

Fig. 3 Temperature dependence of unit cell parameters of the enol-**1** crystal: (a) *a*-axis, (b) *b*-axis, (c) *c*-axis, (d) volume, (e) α-angle, (f) β-angle, and (g) γ-angle. In (c–e and g) the error bars are hidden behind plots. (h) Temperature dependence of the coefficients of thermal expansion (CTEs) of the three axes and the cell volume.

The temperature dependence of the coefficient of thermal expansion (CTE) was determined from the slope of the temperature dependence of the unit cell lengths and the cell volume (Fig. 3h). The CTE of the *a*-axis length increased almost linearly from −116.3 to 84.5 MK^{-1} as the temperature increased from −1.6 to 57.2 °C; the temperature of zero CTE, the inflection point, was 29.2 °C. The CTE of the *c*-axis length was exceptionally large at 356.0 MK^{-1} at −1.6 °C for organic crystals (average ± SD: 71.4 ± 69.9 MK^{-1}),[4] due to the weak interaction between the 1D arrays, as shown in Fig. 2e and f, but decreased with increasing temperature, reaching 159.6 MK^{-1} at 40.4 °C. Then, it increased slightly to 173.7 MK^{-1} at 57.2 °C. The CTE of the *b*-axis length was small at 7.0 MK^{-1} at −1.6 °C, due to the two intermolecular interactions of I and II (Fig. 2e), and then increased to 73.6 MK^{-1} at 57.2 °C. Overall, the volumetric CTE decreased from 364.1 MK^{-1} at −1.6 °C to 250.1 MK^{-1} at 23.6 °C and then increased to 362.2 MK^{-1} at 57.2 °C.

CTE calculated from the slope of the unit cell changes (Fig. 3h) helps to approximately comprehend in which direction the enol-**1** single crystal expands or contracts; however, these values do not necessarily reflect the thermal response of enol-**1** because the unit cell axes do not always match the principal expansion axes.[22a] Then the principal axes and their CTE were calculate by using PASCal.[22b] Fig. 4 and S8† show volume expansion coefficients, principal axes expansion coefficients, and expansivity indicatrices over the temperature range from −1.6 to 23.6 °C (Fig. 4a and d) and from 32.0 to 57.2 °C (Fig. 4c and f). In the temperature range from −1.6 to 23.6 °C, enol-**1** exhibited anisotropic thermal expansion with colossal PTE along the X_3 axis of 329.9 MK^{-1} and NTE along the X_1 axis of −127.7 MK^{-1}, nearly comparable to the CTE values along the *c*- and *a*-axes at −1.6 °C (356.0 and −116.3 MK^{-1}, Fig. 3h), respectively. The X_3 axis corresponds to the direction along which the 1D arrays are stacked *via* weak van der Waals interactions (Fig. 4a, b, d and e); the colossal PTE results from the

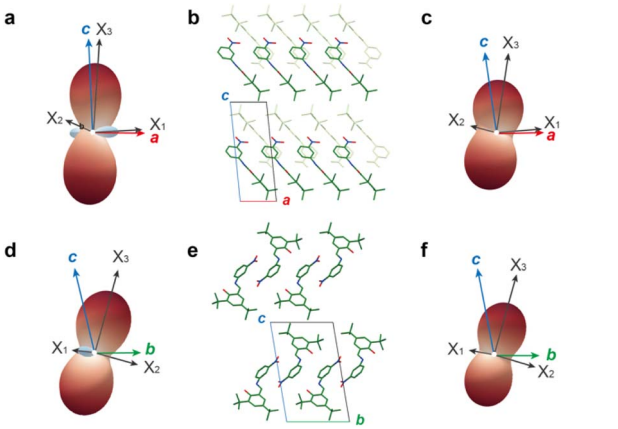

Fig. 4 (a, c, d and f) Expansivity indicatrices obtained from PASCal [22] in the temperature range (a and d) from −1.6 to 23.6 °C and (c and f) from 32.0 to 57.2 °C viewed from the (a and c) (010) and (d and f) (100) faces, respectively. Red and blue represent positive and negative thermal expansion, respectively. (b and e) Molecular packing viewed from the (b) (010) and (e) (100) faces, respectively.

weak interactions along the X_3 direction. The X_1 axis corresponds to the direction along which the *a*-axis is inclined about 20° to the *b*-axis (Fig. 4a and b). In the temperature range from 32.0 to 57.2 °C, the anisotropy becomes less significant since the enol-**1** crystal exhibits PTE in all directions. Similar to the thermal expansion from −1.6 to 23.6 °C, the crystal exhibited colossal CTE of 205.4 MK^{-1} along the X_3 axis (Fig. 4b, c, e and f).

Mechanism of the switch from negative to positive thermal expansion

To elucidate whether the NTE–PTE change in the *a*-axis length (Fig. 3a) is caused by a thermal phase transition or not, differential scanning calorimetry (DSC) measurements were conducted. Any peaks or discontinuous changes in either the heat flow (Fig. S3a–c†) or the heat capacity curves (Fig. S3d†) around 30 °C appeared, clearly indicating that the NTE–PTE change is not derived from a first- or second-order thermal phase transition. Then, the temperature dependence of the molecular conformation, intermolecular interaction, and molecular arrangement was examined in detail (Fig. 5, S4 and S5†). First, to confirm whether or not this NTE–PTE change is caused by intramolecular proton transfer from the enol to the *cis*-keto form and/or disorder of the *tert*-butyl group, the temperature dependence of the C–N distance (Fig. S4b†), C=O distance (Fig. S4c†), difference Fourier maps (Fig. S9†), and occupancy of the disorder (Fig. S4f†) was investigated in detail. No discontinuous changes were observed around 30 °C, suggesting that these two mechanisms are not responsible for the anomalous thermal expansion change.

Then the temperature dependence of intermolecular interactions was investigated. As mentioned in the Crystal structure section, two enol-**1** molecules are connected through a N–O···H–C intermolecular interaction I between the nitro group and Schiff base to form a dimer, and the dimers are connected through a C–H···C–C intermolecular interaction II between the neighboring *tert*-butyl groups along the *b*-axis (Fig. 2e). The lengths of I and II increase due to the weakening of the intermolecular interaction with increasing temperature (Fig. 5d). The dihedral angle (θ, Fig. 5a) between the salicyl and phenyl planes also increases, resulting in a more torsional conformation of the enol-**1** molecule (Fig. 5e). The interplanar distance (*d*, Fig. 5b) extends almost linearly with an increase rate of 7.0×10^{-4} Å °C^{-1} (Fig. 5f). The molecular plane used here is defined as the plane consisting of the Schiff base C–N=C–C and the *para* position C of the phenyl and salicyl rings of two enol-**1** molecules stacked along the *b*-axis (Fig. 5c). In addition, the tilt

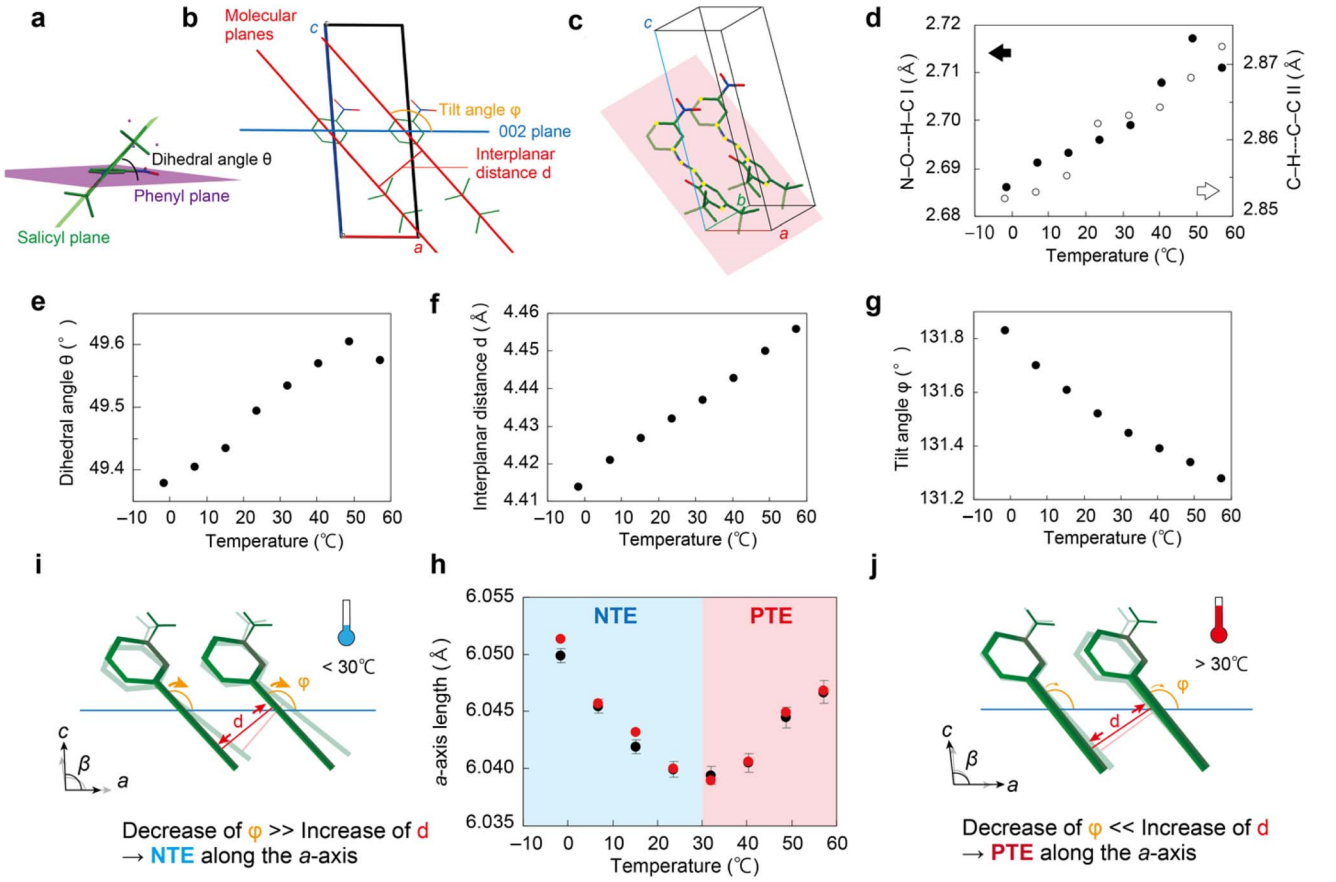

Fig. 5 (a–c) Definitions of (a) dihedral angle θ, (b) interplanar distance *d* and tilt angle φ, and (c) molecular plane. (d–h) Temperature dependences of (d) intermolecular interactions I (solid circles) and II (open circles), (e) dihedral angle θ, (f) interplanar distance *d*, (g) tilt angle φ, and (h) *a*-axis length. Black circles, measured values from the X-ray crystallographic analysis; red circles, calculated from φ and *d*. (i and j) Schematic illustrations of the changes of φ and *d* (i) below and (j) above 30 °C showing NTE and PTE, respectively, along the *a*-axis.

angle (φ, Fig. 5g) of the parallel stacked molecules relative to the *a*-axis decreases; the decrease rate is 0.0121 °C^{-1} from −1.6 to 23.6 °C and declines to 0.0067° °C^{-1} from 32.0 to 57.2 °C (Fig. 5g). We calculated the length along the *a*-axis from *d* and φ (see the details in Fig. S10†) and found it to be in close agreement with the *a*-axis length determined by X-ray crystallographic analysis (Fig. 5h). Thus, geometrical calculations using the temperature dependences of the interplanar distance and the tilt angle reproduced the NTE–PTE switching in *a*-axis thermal expansion.

Calculations were also performed after intentionally changing the temperature dependence of both the interplanar distance *d* and the tilt angle φ as follows (Fig. S11†). If *d* does not increase upon heating, the calculated *a*-axis shows monotonous NTE (blue, Fig. S11a and b†). If the increase rate of *d* is halved (3.5×10^{-4} Å °C^{-1}) from the measured value (7.0×10^{-4} Å °C^{-1}), the calculated *a*-axis also exhibits NTE (green, Fig. S11a and b†). Conversely, when the increase rate is doubled (1.4×10^{-3} Å °C^{-1}), the calculated *a*-axis length displays PTE (red, Fig. S11a and b†). In short, the *a*-axis length shows a NTE to PTE change only when the temperature dependence of *d* is as shown in Fig. 5f.

Moreover, if the tilt angle φ decreases linearly with a decrease rate of 0.0067° °C^{-1} over the entire temperature range, the calculated *a*-axis length exhibits PTE (red, Fig. S11c and d†). By contrast, if the rate of decrease is 0.0121° °C^{-1}, the calculated *a*-axis displays NTE, not PTE (blue, Fig. S11c and d†). When the rate of decrease is reversed, that is, 0.0067° °C^{-1} from −1.6 to 23.6 °C and 0.0121° °C^{-1} from 32.0 to 57.2 °C, the calculated *a*-axis length shows PTE from −1.6 to 23.6 °C and NTE from 32.0 to 57.2 °C (green, Fig. S11c and d†), which is the opposite thermal expansion from the experimental result (Fig. 3a and 5h). Namely, the *a*-axis length shows a NTE to PTE change only when the temperature dependence of φ decreases significantly at low temperatures and decreases less at high temperatures, as seen in Fig. 5g.

Overall, the change in the *a*-axis length of the enol-**1** crystal from NTE to PTE with increasing temperature is due to an exquisite combination of the temperature dependences of both the interplanar distance *d* and the tilt angle φ. At low temperatures, the conformation change represented as the decrease in φ outpaces the increase in *d*, which results in NTE along the *a*-axis (Fig. 5i). By contrast, at high temperatures, the decrease rate of φ becomes less significant, whereas the increase rate of *d* is almost constant. As a result, the increase in *d* becomes dominant, leading to PTE above 30 °C (Fig. 5j).

It has been reported that some elastic molecular crystals show axial PTE due to the change in two parameters, interplanar distance *d* and angle between the molecular plane and the crystallographic axis θ,[23] like the enol-**1** crystal. In contrast to these crystals, enol-**1** show a NTE–PTE switching since the contribution ratio of interplanar distance *d* and tilt angle φ changes below and above 30 °C. Note that the anomalous change of the β-angle, which changes from an increase to

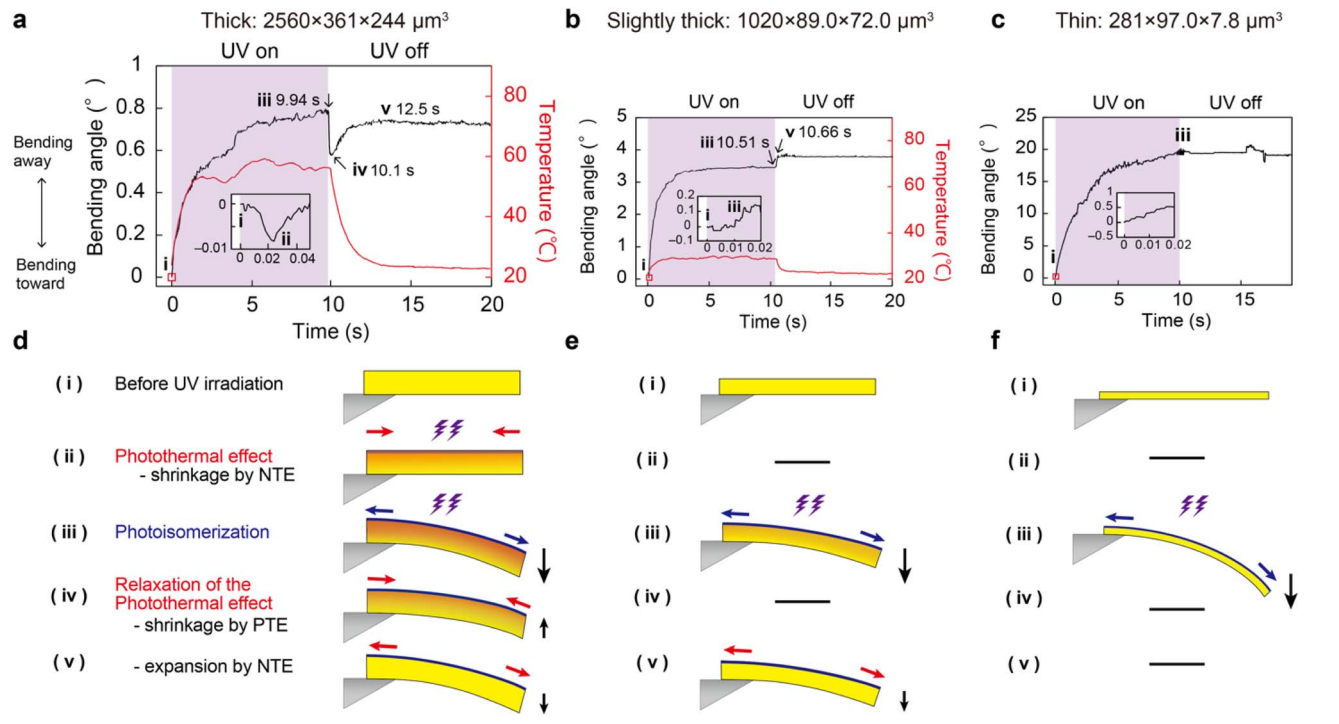

Fig. 6 Photoactuation and the possible mechanisms of enol-**1** crystals upon UV laser (375 nm; 1280 mW cm^{-2}) irradiation. (a and d) Multistep bending of thick crystals, (b and e) two-step bending of slightly thick crystals, and (c and f) one-step bending of thin crystals. (a–c) Time dependence of the bending angle (black) and (a and b) maximum top surface temperature (red). (d–f) Bending mechanisms based on photoisomerisation and the photothermal effect. Blue and red arrows represent expansion/contraction of the top surface by photoisomerisation and the photothermal effect, respectively. In (a), the small, rapid increase in the bending angle and temperature around 4 s might have resulted from the fluctuations in light intensity.

a decrease at 30 °C (Fig. 3f), originates from the combination of the NTE–PTE change of the *a*-axis and the PTE along the *c*-axis.

Photoactuation

We observed photomechanical bending of enol-**1** crystals with its one end fixed upon UV laser irradiation to the top (001)/(00$\bar{1}$) face. Enol-**1** crystals showed three types of bending depending on their thickness (Fig. 6 and S14–S21†).

Multistep bending of thick crystals. When the top face of a thick enol-**1** crystal [length (L): 2560 μm, width (W): 361 μm, and thickness (T): 244 μm] was irradiated with an UV laser, the crystal bent 0.79° away from the light source in 9.94 s due to photoisomerisation (Fig. S12†). Simultaneously the irradiated top surface temperature increased from 24.1 to 56.3 °C by the photothermal effect (Fig. 6a, S17 and Movie S1†). Upon stopping irradiation, the crystal quickly bent forward (0.58°) at 10.1 s, and then gradually bent away again to reach a bending angle of 0.72° at 12.5 s. The mechanism of this multistep bending of the thick crystal can be explained as follows. Upon cessation of UV light irradiation, the top surface temperature decreases through the relaxation of the photothermal effect, and the top surface contracts due to the PTE along the *a*-axis (Fig. 3a), resulting in a bending-up motion [Fig. 6d(iv)]. When the crystal is cooled over the inflection point around 30 °C, the top surface then expands by NTE (Fig. 3a) and the crystal then bends down again [Fig. 6d(v)]. At the early stage (0.02 s) of UV irradiation, the photothermal-driven bending was so small (bending angle: −0.008°) [Fig. 6d(ii)] that it was invisible to the naked eye, because strong photoisomerisation-induced bending offsets photothermal-driven bending [Fig. 6d(iii)].

Such multistep bending occurred in the thick crystals with T > 100 μm (Fig. S14 and S15†) because the top surface temperature rises above 30 °C under UV laser irradiation to cause NTE–PTE switching along the *a*-axis (Fig. S16†). Unlike other salicylideneaniline crystals, for which the threshold for crystal actuation through photoisomerisation is T = 40–100 μm,[15,17] even enol-**1** crystals as thick as 305 μm showed small but significant bending by photoisomerisation because light penetrates deeper into the enol-**1** crystal (7 μm) than other salicylideneaniline crystals (Fig. S13†).[15,17]

Two-step bending of slightly thick crystals. Slightly thick (T = 30–100 μm) crystals also bent through photoisomerisation and the photothermal effect, but multistep bending was not observed (Fig. S14 and S15†). A slightly thick enol-**1** crystal (L = 1020 μm, W = 89.0 μm, and T = 72.0 μm) bent 3.49° away from the light source in 10.51 s due to photoisomerisation, accompanied by a top surface temperature increase from 22.3 to 28.5 °C due to the photothermal effect (Fig. 6b, e, S18, and Movie S2†). When the UV laser was turned off, the top surface temperature decreased through relaxation of the photothermal effect, and the crystal abruptly bent further away (0.44°) at 10.66 s through expansion due to NTE. Immediate bending toward the UV light just after light irradiation was not observed because the maximum top surface temperature did not exceed 30 °C, the NTE–PTE inflection point of thermal expansion along the *a*-axis (Fig. S16†), and only NTE contributed to the photothermal-driven bending.

One-step bending away of thin crystals. Thin (T < 30 μm) crystals bent away due to photoisomerisation alone, in accordance with a previous report (Fig. S14 and S15†).[20] A thin enol-**1** crystal (L = 281 μm, W = 97.0 μm, and T = 7.8 μm) bent 19.4° away from the UV laser *via* photoisomerisation (Fig. 6c, f, S19 and Movie S3†) and retained its bent shape after UV light illumination because of the long lifetime of the *trans*-keto form (τ = 42 days);[20] it returned to its original straight shape reversibly under visible light (520 nm) illumination (Fig. S20†). The photothermal effect did not contribute to the bending of thin crystals, possibly because sufficient thickness and volume are prerequisite for crystal actuation *via* the photothermal effect;[15,17] the threshold for crystal actuation by the photothermal effect (T > 30 μm) was comparable to that of other salicylideneanilines.[15,17]

A few mathematical models reproducing the bending behaviour of photomechanical crystals have been proposed. Chizhik *et al.* reproduced photoisomerisation-driven bending based on rigorous mathematical equations derived from photochemical reactions[11d,g] Monotonous bending of thin enol-**1** crystals through photoisomerisation may be replicated based on these equations. However, reproducing of two-step and multistep bending will be challenging because these equations do not consider the influence of the photothermal effect, for instance, temperature distribution and thermal strain. Naumov *et al.* estimated, on the other hand, crystals' maximum displacement through photoisomerisation using finite element analysis (FEA) by replicating the photoinduced strain through thermal strain.[8e] Our group successfully reproduced the time dependence of photothermal bending by solving the non-steady thermal conduction equation[15,18b,24] and the elastic cantilever beam equation[24] by using FEA. Two-step and multistep bending could be replicated based on a FEA approach rather than mathematical equations derived from photochemical reactions.

Given the NTE–PTE switching at 30 °C, thick crystals are expected to switch their bending behaviour when the temperature was set above 30 °C. Fig. 7 compares the bending of a thick enol-**1** crystal (L = 4593 μm, W = 505 μm, and T = 305 μm) upon UV irradiation at different temperatures. When the temperature was set below 30 °C, like the previous experiments, the top surface temperature increased from 24.0 to 47.8 °C (ΔT = 23.8 °C) by the photothermal effect and the crystal bent 0.25° away from the irradiation direction in 10 s (Fig. 7a and c). When the light was turned off, the crystal quickly bent forward (0.17°) at 10.15 s due to PTE, followed by gradual bending away (0.23° in 14 s) due to NTE (Fig. 7a, c and e). When the temperature was set above 30 °C, the crystal exhibited the same bending away motion (0.24° in 10 s) through photoisomerisation accompanied by the top surface temperature increase from 31.0 to 58.0 °C (ΔT = 27.0 °C). Upon removal of UV light, the crystal quickly bent forward (0.14°) at 10.26 s and did not bend away again, and the bending angles were constants around 0.13 to 0.16° between 10 and 20 s (Fig. 7b and Movie S4†); this would be because the enol-**1** crystal exhibits PTE alone in that temperature range and NTE did not contribute to crystal actuation (Fig. 7d and f). By utilising the NTE–PTE

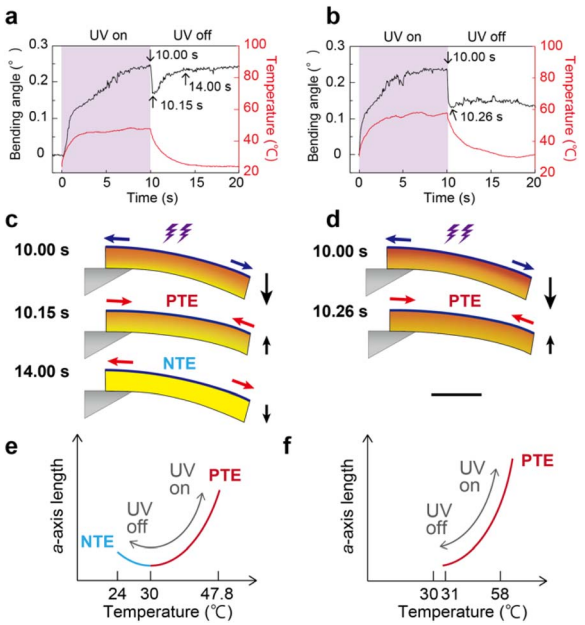

Fig. 7 Photoactuation of a thick enol-**1** crystal (length: 4593 μm, width: 505 μm, and thickness: 305 μm) upon UV laser (375 nm; 317 mW cm^{-2}) irradiation at (a, c and e) 24 °C and (b, d and f) 31 °C. (a and b) Time dependence of the bending angle (black) and maximum top surface temperature (red). (c and d) Bending mechanisms based on photoisomerisation and the photothermal effect. Blue and red arrows represent expansion/contraction of the top surface by photoisomerization and the photothermal effect, respectively. (e and f) Schematic illustrations of the change in the *a*-axis upon UV irradiation.

switching, actuation switching of the same crystal sample under the same irradiation conditions by just tuning atmosphere temperature was realised.

In summary, enol-**1** crystals exhibit three types of bending under light illumination depending on their thickness. (1) Thick (T > 100 μm) crystals show multistep bending due to photoisomerisation and NTE–PTE switching induced by the photothermal effect. (2) Slightly thick (T: 30–100 μm) crystals display two-step bending by photoisomerisation and photothermally induced NTE. (3) Thin (T < 30 μm) crystals bend away monotonously through photoisomerisation alone. Moreover, multistep bending of thick crystals was switched to two-step bending by setting atmosphere temperature above 30 °C.

Conclusions

The crystal of *N*-3,5-di-*tert*-butylsalicylide-3-nitroaniline in the enol form (enol-**1**) exhibits very rare thermal expansion; upon heating, the *a*-axis contracts (NTE) below 30 °C, but then expands (PTE) upon subsequent heating above 30 °C. Detailed analysis of the temperature dependence of the molecular conformation, intermolecular interaction, and molecular arrangement revealed that this switching from NTE to PTE is attributed to two factors: an increase of the interplanar distance and a decrease in the tilt angle of the molecules. Geometric calculations elucidated the mechanism: below 30 °C, the latter factor overwhelms the former, resulting in NTE, whereas above 30 °C, the former overwhelms the latter, resulting in PTE. To our knowledge, enol-**1** is the first organic crystal showing NTE to PTE switching at around room temperature. Upon UV light irradiation of the (001)/(00$\bar{1}$) top face of enol-**1** crystals, thick (>100 μm) crystals showed multistep bending based on NTE and PTE induced by the photothermal effect and photoisomerisation. Slightly thick (30–100 μm) crystals exhibited two-step bending through NTE by the photothermal effect and photoisomerisation. Thin (<30 μm) crystals bent away monotonously through photoisomerisation in accordance with a previous report. We believe that our findings provide not only new insight into organic crystals with NTE–PTE switching without a thermal phase transition but also a strategy for designing crystal actuators showing complex motions upon single light irradiation and switching actuation behaviour depending on atmosphere temperature.

Data availability

All the data supporting this article have been included in the ESI.†

Author contributions

HK conceived the project. YH, SH, and HK designed the experiments. TU synthesised the compound and measured the thickness dependence of the bending motions. SH conducted thermal analysis and measured crystal bending at different temperatures. YH performed X-ray crystallographic analysis. YH, SH, and HK interpreted the results. SH and HK wrote the paper. TA assisted with the project.

Conflicts of interest

There are no conflicts to declare.

Acknowledgements

This research was supported by JSPS Grant-in-Aid for Scientific Research B (17H03107) for H. K., JSPS Research Fellowship for Young Scientists (22J22384 and 21J20125) for S. H. and Y. H., respectively, and the Grant-in-Aid for Young Scientists (Early Bird) at Waseda Research Institute for Science and Engineering for S. H. and Y. H. S. H. and Y. H. thank the Graduate Program for Power Energy Professionals, Waseda University from MEXT WISE Program. The results of ^{1}H NMR, IR, thermal analysis, and X-ray crystallographic analysis were obtained by using equipment shared in the MEXT project for promoting public utilisation of advanced research infrastructure (Program for supporting construction of core facilities), Grant Number JPMXS0440500022.

References

1 N. W. Ashcroft, N. D. Mermin and D. Wei, *Solid State Physics: Revised Edition*, Cengage Learning Asia, Singapore, 2016.

2 (*a*) G. D. Barrera, J. A. O. Bruno, T. H. K. Barron and N. L. Allan, Negative thermal expansion, *J. Phys.: Condens.Matter*, 2005, **17**, R217; (*b*) W. Miller, C. W. Smith, D. S. Mackenzie and K. E. Evans, Negative thermal expansion: a review, *J. Mater. Sci.*, 2009, **44**, 5441–5451; (*c*) C. Lind, Two decades of negative thermal expansion research: where do we stand?, *Materials*, 2012, **5**, 1125–1154; (*d*) N. Shi, Y. Song, X. Xing and J. Chen, Negative thermal expansion in framework structure materials, *Coord. Chem. Rev.*, 2021, **449**, 214204; (*e*) Q. Li, K. Lin, Z. Liu, L. Hu, Y. Cao, J. Chen and X. Xing, Chemical Diversity for Tailoring Negative Thermal Expansion, *Chem. Rev.*, 2022, **122**, 8438–8486.

3 (*a*) Q. Gao, H.-P. Weber, B. M. Craven and R. K. McMullan, Structure of Suberic Acid at 18.4, 75 and 123 K from Neutron Diffraction Data, *Acta Crystallogr., Sect. B*, 1994, **50**, 695–703; (*b*) H. Birkedal, D. Schwarzenbach and P. Pattison, Observation of Uniaxial Negative Thermal Expansion in an Organic Crystal, *Angew. Chem., Int. Ed.*, 2002, **41**, 754; (*c*) S. Haas, B. Batlogg, C. Besnard, M. Schiltz, C. Kloc and T. Siegrist, Large uniaxial negative thermal expansion in pentacene due to steric hindrance, *Phys. Rev. B: Condens. Matter Mater. Phys.*, 2007, **76**, 205203; (*d*) D. Das, T. Jacobs and L. J. Barbour, Exceptionally large positive and negative anisotropic thermal expansion of an organic crystalline material, *Nat. Mater.*, 2010, **9**, 36–39; (*e*) A. D. Fortes, E. Suard and K. S. Knight, Negative Linear Compressibility and Massive Anisotropic Thermal Expansion in Methanol Monohydrate, *Science*, 2011, **331**, 742–746; (*f*) S. Bhattacharya and B. K. Saha, Uniaxial Negative Thermal Expansion in an Organic Complex Caused by Sliding of Layers, *Cryst. Growth Des.*, 2012, **12**, 4716; (*g*) M. Panda, R. Centore, M. Causà, A. Tuzi, F. Borbone and P. Naumov, Strong and Anomalous Thermal Expansion Precedes the Thermosalient Effect in Dynamic Molecular Crystals, *Sci. Rep.*, 2016, **6**, 29610; (*h*) H. Liu, M. J. Gutmann, H. T. Stokes, B. J. Campbell, I. R. Evans and J. S. O. Evans, Supercolossal Uniaxial Negative Thermal Expansion in Chloranilic Acid Pyrazine, CA-Pyz, *Chem. Mater.*, 2019, **31**, 4514–4523.

4 A. van der Lee and D. G. Dumitrescu, Thermal expansion properties of organic crystals: a CSD study, *Chem. Sci.*, 2021, **12**, 8537–8547.

5 (*a*) L. Negi, A. Shrivastava and D. Das, Switching from positive to negative axial thermal expansion in two organic crystalline compounds with similar packing, *Chem. Commun.*, 2018, **54**, 10675; (*b*) S.-Y. Ge, R.-K. Huang, J.-B. Wu, K. Takahashi, C.-S. Lee and T. Nakamura, Planar Positive−Zero−Negative Thermal Expansion Transition in Crystalline Supramolecular Rotors, *Chem. Mater.*, 2023, **35**, 4311–4317.

6 (*a*) *Mechanically Responsive Materials for Soft Robotics*, ed. H. Koshima, Wiley-VCH, Weinheim, 2020; (*b*) H. Koshima, S. Hasebe, Y. Hagiwara and T. Asahi, Mechanically Responsive Organic Crystals by Light, *Isr. J. Chem.*, 2021, **61**, 683–696; (*c*) Y. Huang, Q. Gong and J. Yu, Organic crystal-based flexible smart materials, *Sci. China Mater.*, 2022, **65**, 1994–2016; (*d*) W. M. Awad, D. W. Davies, D. Kitagawa, J. M. Halabi, M. B. Al-Handawi, I. Tahir, F. Tong, G. Campillo-Alvarado, A. G. Shtukenberg, T. Alkhidir, Y. Hagiwara, M. Almehairbi, L. Lan, S. Hasebe, D. P. Karothu, S. Mohamed, H. Koshima, S. Kobatake, Y. Diao, R. Chandrasekar, H. Zhang, C. C. Sun, C. Bardeen, R. O. Al-Kaysi, B. Kahr and P. Naumov, Mechanical properties and peculiarities of molecular crystals, *Chem. Soc. Rev.*, 2023, **52**, 3098–3169.

7 (*a*) S. Kobatake, S. Takami, H. Muto, T. Ishikawa and M. Irie, Rapid and reversible shape changes of molecular crystals on photoirradiation, *Nature*, 2007, **446**, 778–781; (*b*) M. Irie, T. Fukaminato, K. Matsuda and S. Kobatake, Photochromism of Diarylethene Molecules and Crystals: Memories, Switches, and Actuators, *Chem. Rev.*, 2014, **114**, 12174–12277; (*c*) M. Irie, *Diarylethene Molecular Photoswitches*, Wiley-VCH, Weinheim, 2021.

8 (*a*) H. Koshima, N. Ojima and H. Uchimoto, Mechanical Motion of Azobenzene Crystals upon Photoirradiation, *J. Am. Chem. Soc.*, 2009, **131**, 6890–6891; (*b*) O. S. Bushuyev, T. A. Singleton and C. J. Barrett, Fast, Reversible, and General Photomechanical Motion in Single Crystals of Various Azo Compounds Using Visible Light, *Adv. Mater.*, 2013, **25**, 1796–1800; (*c*) T. Taniguchi, T. Asahi and H. Koshima, Photomechanical Azobenzene Crystals, *Crystals*, 2019, **9**, 437; (*d*) Y. Hao, L. Gao, X. Zhang, L. Wei, T. Wang, N. Wang, X. Huang, H. Yu and H. Hao, Azobenzene crystal polymorphism enables tunable photoinduced deformations, mechanical behaviours and photoluminescence properties, *J. Mater. Chem. C*, 2021, **9**, 8294–8301; (*e*) J. M. Halabi, E. Ahmed, S. Sofela and P. Naumov, Performance of molecular crystals in conversion of light to mechanical work, *Proc. Natl. Acad. Sci. U. S. A.*, 2021, **118**, e2020604118; (*f*) A. K. Bartholomew, I. B. Stone, M. L. Steigerwald, T. H. Lambert and X. Roy, Highly Twisted Azobenzene Ligand Causes Crystals to Continuously Roll in Sunlight, *J. Am. Chem. Soc.*, 2022, **144**, 16773–16777.

9 (*a*) R. O. Al-Kaysi and C. J. Bardeen, Reversible Photoinduced Shape Changes of Crystalline Organic Nanorods, *Adv. Mater.*, 2007, **19**, 1276–1280; (*b*) L. Zhu, R. O. Al-Kaysi and C. J. Bardeen, Reversible Photoinduced Twisting of Molecular Crystal Microribbons, *J. Am. Chem. Soc.*, 2011, **133**, 12569–12575; (*c*) T. Kim, L. Zhu, L. J. Mueller and C. J. Bardeen, Mechanism of Photoinduced Bending and Twisting in Crystalline Microneedles and Microribbons Composed of 9-Methylanthracene, *J. Am. Chem. Soc.*, 2014, **136**, 6617–6625; (*d*) Y.-S. Chen, C.-H. Wang, Y.-H. Hu, C.-Y. D. Lu and J.-S. Yang, An Elastic Organic Crystal Enables Macroscopic Photoinduced Crystal Elongation, *J. Am. Chem. Soc.*, 2023, **145**, 6024–6028.

10 (*a*) H. Koshima, R. Matsuo, M. Matsudomi, Y. Uemura and M. Shiro, Light-Driven Bending Crystals of Salicylidenephenylethylamines in Enantiomeric and Racemate Forms, *Cryst. Growth Des.*, 2013, **13**, 4330–4337; (*b*) A. Takanabe, M. Tanaka, K. Johmoto, H. Uekusa,

T. Mori, H. Koshima and T. Asahi, Optical Activity and Optical Anisotropy in Photomechanical Crystals of Chiral Salicylidenephenylethylamines, *J. Am. Chem. Soc.*, 2016, **138**, 15066–15077.

11 (*a*) G. A. Abakumov and V. I. Nevodchikov, Thermo- and Photomechanical Effects on Crystals of a Free-Radical Complex, *Dokl. Phys. Chem.*, 1982, **266**, 1407–1410; (*b*) E. V. Boldyreva, A. A. Sidelnikov, A. P. Chupakhin, N. Z. Lyakhov and V. V. Boldyrev, Deformation and Mechanical Fragmentation of the Crystals $[Co(NH_3)_5NO_2]X_2$ (X = Cl, Br, NO_3) in the Course of Linkage Photoisomerisation, *Dokl. Phys. Chem.*, 1984, **277**, 893–896; (*c*) P. Naumov, S. C. Sahoo, B. A. Zakharov and E. V. Boldyreva, Dynamic Single Crystals: Kinematic Analysis of Photoinduced Crystal Jumping (The Photosalient Effect), *Angew. Chem., Int. Ed.*, 2013, **52**, 9990–9995; (*d*) S. Chizhik, A. Sidelnikov, B. Zakharov, P. Naumov and E. Boldyreva, Quantification of photoinduced bending of dynamic molecular crystals: from macroscopic strain to kinetic constants and activation energies, *Chem. Sci.*, 2018, **9**, 2319–2335; (*e*) R. Samanta, S. Ghosh, R. Devarapalli and C. M. Reddy, Visible Light Mediated Photopolymerization in Single Crystals: Photomechanical Bending and Thermomechanical Unbending, *Chem. Mater.*, 2018, **30**, 577–581; (*f*) P. Gupta, T. Panda, S. Allu, S. Borah, A. Baishya, A. Gunnam, A. Nangia, P. Naumov and N. K. Nath, Crystalline Acylhydrazone Photoswitches with Multiple Mechanical Responses, *Cryst. Growth Des.*, 2019, **19**, 3039–3044; (*g*) E. Ahmed, S. Chizhik, A. Sidelnikov, E. Boldyreva and P. Naumov, Relating Excited States to the Dynamics of Macroscopic Strain in Photoresponsive Crystals, *Inorg. Chem.*, 2022, **61**, 3573–3585.

12 (*a*) S. C. Sahoo, M. K. Panda, N. K. Nath and P. Naumov, Biomimetic Crystalline Actuators: Structure–Kinematic Aspects of the Self-Actuation and Motility of Thermosalient Crystals, *J. Am. Chem. Soc.*, 2013, **135**, 12241–12251; (*b*) Z. S. Yao, M. Mito, T. Kamachi, Y. Shiota, K. Yoshizawa, N. Azuma, Y. Miyazaki, K. Takahashi, K. Zhang, T. Nakanishi, S. Kang, S. Kanegawa and O. Sato, Molecular motor-driven abrupt anisotropic shape change in a single crystal of a Ni complex, *Nat. Chem.*, 2014, **6**, 1079–1083; (*c*) S. Q. Su, T. Kamachi, Z. S. Yao, Y. G. Huang, Y. Shiota, K. Yoshizawa, N. Azuma, Y. Miyazaki, M. Nakano, G. Maruta, S. Takeda, S. Kang, S. Kanegawa and O. Sato, Assembling an alkyl rotor to access abrupt and reversible crystalline deformation of a cobalt(II) complex, *Nat. Commun.*, 2015, **6**, 8810; (*d*) T. Taniguchi, H. Sugiyama, H. Uekusa, M. Shiro, T. Asahi and H. Koshima, Walking and rolling of crystals induced thermally by phase transition, *Nat. Commun.*, 2018, **9**, 538.

13 (*a*) T. Klaser, J. Popović, J. A. Fernandes, S. C. Tarantino, M. Zema and Ž. Skoko, Does Thermosalient Effect Have to Concur with a Polymorphic Phase Transition? The Case of Methscopolamine Bromide, *Crystals*, 2018, **8**, 301; (*b*) M. Jin, S. Yamamoto, T. Seki, H. Ito and M. A. Garcia-Garibay, Anisotropic Thermal Expansion as the Source of Macroscopic and Molecular Scale Motion in Phosphorescent Amphidynamic Crystals, *Angew. Chem., Int. Ed.*, 2019, **58**, 18003–18010; (*c*) T. Seki, T. Mashimo and H. Ito, Crystal Jumping of Simple Hydrocarbons: Cooling-induced Salient Effect of Bis-, Tri-, and Tetraphenylethene through Anisotropic Lattice Dimension Changes without Thermal Phase Transitions, *Chem. Lett.*, 2020, **49**, 174–177; (*d*) Y. Miura, T. Takeda, N. Yoshioka and T. Akutagawa, Thermosalient Effect of 5-Fluorobenzoyl-4-(4-methoxyphenyl)ethynyl-1-methylimidazole without Phase Transition, *Cryst. Growth Des.*, 2022, **22**, 5904–5911.

14 Y. Hagiwara, T. Taniguchi, T. Asahi and H. Koshima, Crystal actuator based on a thermal phase transition and photothermal effect, *J. Mater. Chem. C*, 2020, **8**, 4876–4884.

15 S. Hasebe, Y. Hagiwara, J. Komiya, M. Ryu, H. Fujisawa, J. Morikawa, T. Katayama, D. Yamanaka, A. Furube, H. Sato, T. Asahi and H. Koshima, Photothermally Driven High-Speed Crystal Actuation and Its Simulation, *J. Am. Chem. Soc.*, 2021, **143**, 8866–8877.

16 S. Hasebe, Y. Hagiwara, K. Takechi, T. Katayama, A. Furube, T. Asahi and H. Koshima, Polymorph-Derived Diversification of Crystal Actuation by Photoisomerisation and the Photothermal Effect, *Chem. Mater.*, 2022, **34**, 1315–1324.

17 S. Hasebe, Y. Hagiwara, K. Hirata, T. Asahi and H. Koshima, Crystal actuation switching by crystal thickness and light wavelength, *Mater. Adv.*, 2022, **3**, 7098–7106.

18 (*a*) X. Yang, L. Lan, L. Li, J. Yu, X. Liu, Y. Tao, Q.-H. Yang, P. Naumov and H. Zhang, Collective photothermal bending of flexible organic crystals modified with MXene-polymer multilayers as optical waveguide arrays, *Nat. Commun.*, 2023, **14**, 3627; (*b*) D. W. Kim, Y. Hagiwara, S. Hasebe, M. O. Dogan, M. Zhang, T. Asahi, H. Koshima and M. Sitti, Broad-Wavelength Light-Driven High-Speed Hybrid Crystal Actuators Actuated Inside Tissue-Like Phantoms, *Adv. Funct. Mater.*, 2023, 2305916.

19 (*a*) E. Hadjoudis and I. M. Mavridis, Photochromism and thermochromism of Schiff bases in the solid state: structural aspects, *Chem. Soc. Rev.*, 2004, **33**, 579–588; (*b*) K. Amimoto and T. Kawato, Photochromism of organic compounds in the crystal state, *J. Photochem. Photobiol., C*, 2005, **6**, 207–226.

20 H. Koshima, K. Takechi, H. Uchimoto, M. Shiro and D. Hashizume, Photomechanical bending of salicylideneaniline crystals, *Chem. Commun.*, 2011, **47**, 11423–11425.

21 J. Harada, H. Uekusa and Y. Ohashi, X-ray Analysis of Structural Changes in Photochromic Salicylideneaniline Crystals. Solid-State Reaction Induced by Two-Photon Excitation, *J. Am. Chem. Soc.*, 1999, **121**, 5809–5810.

22 (*a*) M. J. Cliffe and A. L. Goodwin, PASCal: a principal axis strain calculator for thermal expansion and compressibility determination, *J. Appl. Crystallogr.*, 2012, **45**, 1321–1329; (*b*) M. Lertkiattrakul, M. L. Evans and M. J. Cliffe, PASCal Python: A Principal Axis Strain Calculator, *J. Open Source Softw.*, 2023, **8**, 5556.

23 (*a*) J. Brock, J. J. Whittaker, J. A. Powell, M. C. Pfrunder, A. Grosjean, S. Parsons, J. C. McMurtrie and J. K. Clegg,

Elastically Flexible Crystals have Disparate Mechanisms of Molecular Movement Induced by Strain and Heat, *Angew. Chem., Int. Ed.*, 2018, **57**, 11325–11328; (*b*) S. A. Rather and B. K. Saha, Thermal Expansion Study as a Tool to Understand the Bending Mechanism in a Crystal, *Cryst. Growth Des.*, 2018, **18**, 2712–2716; (*c*) S. A. Rather and B. K. Saha, Understanding the elastic bending mechanism in a 9,10-anthraquinone crystal through thermal expansion study, *CrystEngComm*, 2021, **23**, 5768–5773.

24 Y. Hagiwara, S. Hasebe, H. Fujisawa, J. Morikawa, T. Asahi and H. Koshima, Photothermally induced natural vibration for versatile and high-speed actuation of crystals, *Nat. Commun.*, 2023, **14**, 1354.